I. SZANYI,[1] V. SVINTOZELSKYI[2]

[1] Eötvös Loránd University
 (1/A, Pázmány Péter Walkway, 1117 Budapest, Hungary; e-mail: istvan.szanyi@cern.ch)
[2] Taras Shevchenko National University of Kyiv
 (64/13, Volodymyrska Str., Kyiv 01601, Ukraine; e-mail: 1vladimirsw@gmail.com)

POMERON-POMERON SCATTERING

The central exclusive diffractive (CED) production of meson resonances potentially is a factory producing new particles, in particular, a glueball. The produced resonances lie on trajectories with vacuum quantum numbers, essentially on the pomeron trajectory. A tower of resonance recurrences, the production cross-section, and the resonances widths are predicted. A new feature is the form of a non-linear pomeron trajectory, producing resonances (glueballs) with increasing widths. At LHC energies, in the nearly forward direction, the t-channel both in elastic, single, or double diffraction dissociations, as well as in CED, is dominated by the pomeron exchange (the role of secondary trajectories is negligible, however a small contribution from the odderon may be present).

K e y w o r d s: Regge trajectory, pomeron, glueball, CED, LHC.

1. Introduction

The central exclusive diffractive (CED) production continues attracting attention of both theorists and experimentalists (see, e.g., [1] and references therein). Interest in this subject is triggered by LHC's high energies, where even the subenergies at an equal partition is sufficient to neglect the contribution from secondary Regge trajectories. Consequently, CED can be considered as a gluon factory to produce exotic particles such as glueballs.

Below, we will study CED shown in Fig. 1 with topology 4. Its knowledge is essential in studies with diffractive excited protons, topologies 5 and 6.

In the single-diffraction dissociation or single dissociation (SD), one of the incoming protons dissociates (topology 2 in Fig. 1), in double-diffraction dissociation or double dissociation (DD), both protons dissociate (topology 3), and, in central dissociation (CD) or double-Pomeron exchange (DPE), none of the protons dissociates (topology 4). These processes are tabulated below as

SD $pp \rightarrow Xp$
or $pp \rightarrow pY$
DD $pp \rightarrow XY$
CD (DPE) $pp \rightarrow pXp$,

where X and Y represent diffractive dissociated protons.

2. Pomeron/Glueball Trajectory

Regge trajectories $\alpha(s)$ connect the scattering region, $s < 0$, with that of particle spectroscopy, $s > 0$. In this way, they realize the crossing symmetry and anticipate the duality, *i.e.*, the dynamics of two kinematically disconnected regions is intimately related: the trajectory at $s < 0$ should "know" its behavior in the cross channel and vice versa. Most of the familiar meson and baryon trajectories follow the above regularity: with their parameters fitted in the scattering region, they fit the masses and spins of relevant resonances, see, e.g., [2]. The behavior of trajectories both in the scattering and particle regions is close to linear, which is an approximation to reality. Resonances on real and linear trajectories imply unrealistic infinitely narrow resonances. Analyticity and unitarity also require that the trajectories be non-linear complex functions [3,4]. Constraints on the threshold and asymptotic behaviors of Regge trajectories were derived from dual amplitudes with Mandelstam analyticity [4]. Accordingly, near the threshold (see also [5–7])

$$\Im m\alpha(s)_{s \rightarrow s_0} \sim (s - s_0)^{\alpha(s_0)+1/2}, \qquad (1)$$

while the trajectories are constrained asymptotically by [4]

$$\left| \frac{\alpha(s)}{\sqrt{s} \ln s} \right|_{s \to \infty} \leq \text{const.} \tag{2}$$

The above asymptotic constrain can be still lowered to a logarithm by imposing (see [8] and earlier references) the wide-angle power behavior for the amplitude.

The above constrains are restrictive, but still leave much room for the model building. In Refs. [9, 10], the imaginary part of the trajectories (resonances' widths) was recovered from the nearly linear real part of the trajectory by means of dispersion relations and fits to the data.

While the parameters of meson and baryon trajectories can be determined both from the scattering data and from the particle spectra, this is not true for the pomeron (and odderon) trajectory, known from fits to scattering data only (negative values of its argument). An obvious task is to extrapolate the pomeron trajectory from negative to positive values to predict glueball states at $J = 2, 4, \ldots$ was not solved. Given the nearly linear form of the pomeron trajectory, known from the fits to the (exponential) diffraction cone, little room is left for variations in the region of particles ($s > 0$.) The non-observability of any glueball state in the expected values of spins and masses may have two explanations: 1. glueballs appear as hybrid states mixed with quarks, which makes their identification difficult; 2. their production cross-section is low and their widths is large. To resolve these problems, one needs a reliable model to predict cross-sections and decay widths of the expected glueballs, in which the pomeron trajectory plays a crucial role.

Models for the pomeron/glueball trajectories were proposed and discussed in quite a number of papers [11–14]. They range from simple phenomenological (also linear) models to quite sophisticated ones, involving QCD, lattice calculations, extra dimensions, etc. The basic problem of the production cross-sections and the decay widths of produced glueballs in the cited papers remains open. Close to the spirit of the present approach are papers [12–14], where the pomeron/glueball trajectory, including the threshold singularities is manifestly non-linear, and the real part terminates.
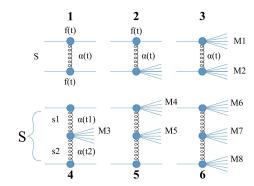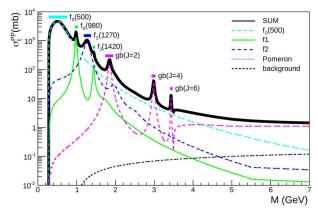

Fig. 1. Regge-pole factorization

Fig. 2. Pomeron-pomeron total cross-section in CED calculated in Ref. [1]

We continue the lines of researches initiated in Refs. [1, 15] in which an analytic pomeron trajectory was used to calculate the pomeron-pomeron cross-section in the central exclusive production measurable in the proton-proton scattering, e.g., at the LHC. The basic idea in that approach is the use of a non-linear complex Regge trajectory for the pomeron satisfying the requirements of the analytic S-matrix theory and fitting the data. Fits imply high-energy elastic proton-proton scattering data. For the scattering amplitude, the simple and efficient Donnachie–Landshoff model [16] was used. The essential difference with respect to many similar studies lies in the non-linear behavior of the trajectories. They affect crucially the predicted properties of the resonances. Our previous papers [1, 15] contain more than that: the fitted trajectories are used to calculate pomeron-pomeron scattering cross-sections in the central exclusive diffraction at the LHC. Figure 2 shows the result of those calculations.

Papers [1, 15] contain detailed analyses and fits of both the pomeron and non-leading (also complex!) Regge trajectories, the emphases being on the pomeron/gluon one. In the present study, we revise the basic object, namely the model of a pomeron trajectory, postponing other details (secondary reggeons, CED, *etc.*) to a forthcoming study.

2.1. Scattering amplitude, cross-sections, resonances

In Ref. [1], the contribution of resonances to the pomeron-pomeron (PP) cross-section was calculated from the imaginary part of the amplitude with the use of the optical theorem:

$$\sigma_t^{PP}(M^2) = \Im m\, A(M^2, t = 0) =$$

$$= a \sum_{i=f,P} \sum_J \frac{[f_i(0)]^{J+2}\, \Im m\, \alpha_i(M^2)}{(J - \Re e\, \alpha_i(M^2))^2 + (\Im m\, \alpha_i(M^2))^2}. \tag{3}$$

In this section, we concentrate on the pomeron. In this case, Eq. (3) reduces to

$$\sigma_t^{PP}(M^2) = a \sum_J \frac{k^{J+2}\, \Im m\, \alpha(M^2)}{(J - \Re e\, \alpha(M^2))^2 + (\Im m\, \alpha(M^2))^2}, \tag{4}$$

where $k = f_i(0)$, and, for simplicity, we set $k = 1$.

We start by comparing the resulting glueball spectra in two ways: first, we plot the real and imaginary parts of the trajectory (Chew–Frautchi plot) and calculate the resonances' widths by using the relation (see, e.g., Eq. (18) in [15])

$$\Gamma(s = M^2) = \frac{2\Im m \alpha(s)}{|\alpha'(s)|}, \tag{5}$$

where $\alpha'(s) = d\Re e\alpha(\sqrt{s})/d\sqrt{s}$.

2.2. Analytic Regge trajectories

In the previous studies [1, 15, 18], the following two types of trajectories were considered:

$$\alpha(s) = \alpha_0 + \alpha_1 s + \alpha_2(\sqrt{s_0 - s} - \sqrt{s_0}), \tag{6}$$

and

$$\alpha(s) = \alpha_0 + \alpha_2(\sqrt{s_0 - s} - \sqrt{s_0}) + \alpha_3(\sqrt{s_1 - s} - \sqrt{s_1}), \tag{7}$$

In trajectory Eq. (7), the second, heavy threshold was introduced to mimic the nearly linear rise of the trajectory for $s < s_1$, avoiding an indefinite rise as in Eq. (6), thus securing the asymptotic square-root upper bound (2). As realized in Refs. [1, 15], these trajectories result in "narrowing" the resonances (here, a glueball) whose widths decrease, as their masses increase. Below, we show that this deficiency is remedied in a trajectory that satisfies the constraint of the analytic S-matrix theory, namely, the threshold behavior and asymptotic boundedness, and produces fading resonances (glueballs), whose widths are rising with mass.

The trajectory is:

$$\alpha(s) = \frac{a + bs}{1 + c(\sqrt{s_0 - s} - \sqrt{s_0})}, \tag{8}$$

where $s_0 = 4m_\pi^2$, and a, b, c are adjustable parameters, to be fitted to scattering ($s < 0$) data with the obvious constraints: $\alpha(0) \approx 1.08$ and $\alpha'(0) \approx 0.3$. Trajectory Eq. (8) has square-root asymptotic behavior, in accord with the requirements of the analytic S-matrix theory.

With the parameters fitted in the scattering region, we continue trajectory Eq. (8) to positive values of s. When approaching the branch cut at $s = s_0$, one has to choose the right Riemann sheet, For the $s > s_0$ trajectory Eq. (8) may be rewritten as

$$\alpha(s) = \frac{a + bs}{1 - c(i\sqrt{s - s_0} + \sqrt{s_0})} \tag{9}$$

with the sign "minus" in front of c, according to the definition of the physical sheet.

For $s \gg s_0, |\alpha(s)| \to \frac{b}{c}\sqrt{|s|}$. For $s > s_0$ (on the upper edge of the cut), $\Im m\, \alpha > 0$.

The intercept is $\alpha(0) = a$, and the slope at $s = 0$ is

$$\alpha'(0) = b + \frac{ac}{2\sqrt{s_0}}. \tag{10}$$

To anticipate subsequent fits and discussions, we note that the presence of the light threshold $s_0 = 4m_\pi^2$ (required by unitarity and the observed "break" in the data) results in the increasing, compared with the "standard" value of ≈ 0.25 GeV^{-2}, intercept.

2.3. Simple Regge-pole fits to high-energy elastic scattering data

High-energy elastic proton-proton and proton-antiproton scatterings, including ISR and LHC energies,

were successfully fitted with non-linear pomeron trajectories Eqs. (6) and (7) in a number of papers, see [17] and references therein. Here, we are interested in the parametrization of the pomeron (and odderon) trajectories, dominating the LHC energy region, and concentrate on the LHC data, where the secondary trajectories can be completely ignored in the near forward direction.

At lower energies (e.g., at the ISR), the diffraction cone shows the almost perfect exponential behavior corresponding to a linear pomeron trajectory in a wide span of $0 < -t < 1.3$ GeV^2, which is violated only by the "break" near $t \approx -0.1$ GeV^2. At the LCH, it is almost immediately followed by another structure, namely, by the dip at $t \approx -0.6$ GeV^2. The dynamics of the dip (diffraction minimum) has been treated fully and successfully [18]. However, those details are irrelevant to the behavior of the pomeron trajectory in the resonance (positive s) region and the expected glueballs there, that depend largely on the imaginary part of the trajectory and basically on the threshold singularity in Eq. (8).

In Fig. 3, we show a fit to the low-$|t|$ elastic proton-proton differential cross-section data [19] at 13 TeV with a simple model:

$$A_P(s,t) = a_P e^{b_P t} e^{-i\pi\alpha_P(t)/2}(s/s_{0P})^{\alpha_P(t)}, \qquad (11)$$

where $\alpha_P(t)$ is given by Eq. (8) (changing the variable s to the variable t).
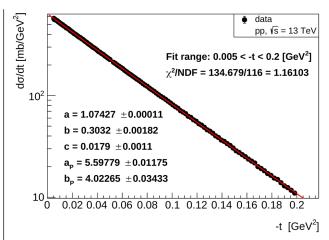
We used the norm

$$\frac{d\sigma}{dt} = \frac{\pi}{s^2}|A_P(s,t)|^2. \qquad (12)$$

Figure 4 shows the normalized form of the differential cross-section (used by TOTEM [19]) illustrating the low-$|t|$ "break" phenomenon [17] related to the non-linear square-root term in the pomeron trajectory. However, it should be also noted that the "break" may be resulted from the two-pion threshold both in the trajectory and the non-exponential residue, as discussed in [17].

2.4. Extrapolating the pomeron trajectory to the resonance region, $s > 0$

Fitting to the measured pp scattering data, the values of the pomeron trajectory parameters became known. Changing back the variable t to the variable s (crossing symmetry), we can extrapolate now the

Fig. 3. Fitted pp differential cross-section at 13 TeV using amplitude Eq. (11) and trajectory Eq. (8)
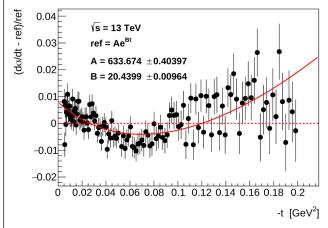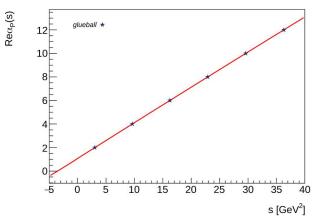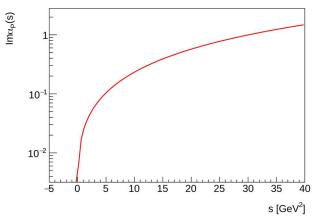
Fig. 4. Normalized form of the fitted pp differential cross-section at 13 TeV using amplitude Eq. (11) and trajectory Eq. (8)

Fig. 5. Real part of the pomeron trajectory Eq. (8) as a function of s

Fig. 6. Imaginary part of the pomeron trajectory Eq. (8) as a function of s
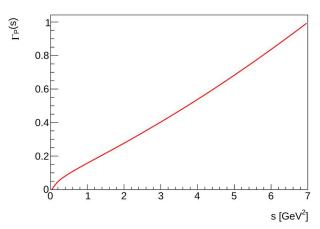

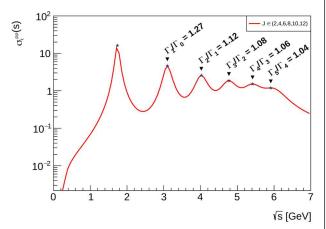**Fig. 7.** Resonance width Eq. (5) calculated with trajectory Eq. (8)

Fig. 8. Pomeron-pomeron total cross-section Eq. (4) (setting $a = 1$ and $J \in (2, 4, 6, 8, 10, 12)$) calculated with trajectory Eq. (8) showing also the ratios of neighboring resonances' widths

pomeron trajectory to the resonance region, $s > 0$. Figures 5 and 6 show, respectively, the real and imaginary parts of the trajectories (during the calculations, the trajectory parameter values are taken from the fit shown in Fig. 3). Figure 5 shows the glueball spectra lying on the pomeron trajectory. Such glueballs have even integer spins ($J \equiv \operatorname{Re} \alpha_P(s) = 2, 4, 6, ...$) and mass square $M^2 = s$.

In Figs. 8 and 7, we can see, respectively, the resonance width and the pomeron-pomeron total cross section.

3. Summary

Using a simple pomeron pole model fit to the 13-TeV pp low-$|t|$ differential cross-section data, we have extrapolated the pomeron trajectory from negative to positive values to predict glueball states at $J = 2, 4, 6, 8, 10,$ and 12. We have predicted also the cross-sections and decay widths of the expected glueballs. Applying the pomeron trajectory Eq. (8), we have obtained such resonances (glueballs) whose widths increase with their masses.

1. R. Fiore, L. Jenkovszky, R. Schicker. Exclusive diffractive resonance production in proton-proton collisions at high energies. *Eur. Phys. J. C* **78**, 468 (2018).

2. P.D.B. Collins. *An Introduction to Regge Theory and High Energy Physics* (Cambridge Univ. Press, 1977).

3. A. Degasperis, E. Predazzi. Dynamical calculation of Regge trajectories. *Nuovo Cimento A* **65**, 764 (1970).

4. A.I. Bugrij, G. Cohen-Tannoudji, L.L. Jenkovszky, N.A. Kobylinsky. Dual amplitudes with Mandelstam analyticity. *Fortschritte der Physik* **21**, 427 (1973).

5. A.O. Barut, D.E. Zwanziger. Complex angular momentum in relativistic S-matrix theory. *Phys. Rev.* **127**, 974 (1962).

6. V.N. Gribov, Ya.I. Pomeranchuk. Properties of the elastic scattering amplitude at high energies. *Nucl. Phys.* **38**, 516 (1962).

7. R. Oehme. Complex angular momentum in elementary particle scattering, in *Proceedings of the Scottish Universities Summer School* Edinburgh 1963, edited by R. G. Moorhouse, p.129 (1964).

8. L.L. Jenkovszky. High-energy elastic hadron scattering. *La Rivista del Nuovo Cimento* **10**, 1 (1987).

9. R. Fiore, L.L. Jenkovszky, F. Paccanoni, A. Prokudin. Baryonic Regge trajectories with analyticity constraints. *Phys. Rev. D* **70**, 054003 (2004).

10. R. Fiore, L.L. Jenkovszky, V. Magas, F. Paccanoni, A. Papa. Analytic model of Regge trajectories. *Eur. Phys. J. A* **10**, 217 (2001).

11. M.N. Sergeenko. Gluonium states and the Pomeron trajectory. arXiv:0807.0911.

12. M.M. Brisudova, L. Burakovsky, T. Goldman, A. Szczepaniak. Nonlinear Regge trajectories and glueballs. arXiv:nucl-th/0303012.

13. T. Goldman, A. Szczepaniak. Nonlinear Regge trajectories and glueballs. arXiv:hep-ph/0009126.

14. M.M. Brisudova, L. Burakovsky, T. Goldman. Spectroscopy "windows" of quark-antiquark mesons and glueballs with effective Regge trajectories. arXiv:hep-ph/0008212.

15. R. Fiore, L. Jenkovszky, R. Schicker. Resonance production in Pomeron–Pomeron collisions at the LHC. *Eur. Phys. J. C* **76**, 38 (2016).

16. A. Donnachie, P.V. Landshoff. Hard diffraction: Production of high pT jets, W or Z, and Drell–Yan pairs. *Nucl. Phys. B* **303**, 634 (1988).

17. L. Jenkovszky, I. Szanyi, CI. Tan. Shape of proton and the pion cloud. *Eur. Phys. J. A* **54**, 116 (2018).

18. I. Szanyi, N. Bence, L. Jenkovszky. New physics from TOTEM's recent measurements of elastic and total cross-sections. *J. Phys. G: Nucl. Part. Phys.* **46**, 055002 (2019).

19. The TOTEM collaboration. First determination of the ρ parameter at $\sqrt{s} = 13$ TeV – probing the existence of a colourless three-gluon bound state. arXiv:1812.04732.

I. Сані, В. Свінтозельський

ПОМЕРОН-ПОМЕРОННЕ РОЗСІЮВАННЯ

Р е з ю м е

Центральне ексклюзивне дифракційне (ЦЕД) народження мезонних резонансів потенційно може бути фабрикою нових частинок, зокрема глюболів. Отримані резонанси лягають на траєкторії з вакуумними квантовими числами, переважно на траєкторію померона. Отримано ширини резонансів та їхній поперечний переріз. Новою особливістю є використання нелінійної траєкторії для померона, що продукує резонанси (глюболи) зі зростаючою шириною. При енергіях ВАК, у майже прямому напрямку в t-каналі як при пружних – одинарної чи подвійної дифракційної дисоціації, так і в ЦЕД домінує обмін померонами (вплив вторинних траєкторій нехтовний, хоча можливе врахування невеликого внеску оддерона).